Theor Chem Acc (2012) 131:1132
DOI 10.1007/s00214-012-1132-z

REGULAR ARTICLE

A distributed point polarizable force field for carbon dioxide

Fang-Fang Wang · Revati Kumar · Kenneth D. Jordan

Received: 14 June 2011 / Accepted: 19 August 2011 / Published online: 2 March 2012

Abstract A distributed point polarizable model potential for carbon dioxide, with explicit terms for charge penetration and induction, is introduced. This model potential accurately describes the structures and interaction energies of small $(CO_2)_n$ clusters and also gives the second virial coefficients and radial distribution functions of supercritical CO_2 in excellent agreement with experiment.

Keywords Carbon dioxide · Force field · Charge penetration · Polarization · Symmetry-adapted perturbation theory

1 Introduction

Carbon dioxide (CO_2) has attracted considerable attention because of its use as a supercritical fluid for extraction processes and because of its role as a greenhouse gas. Not surprising, there have been many of computer simulations of CO_2 in the condensed phase as well as in a range of chemical environments. Most of these simulations have been carried out in model potentials, and, as a result, the success of such simulations depends on the quality of the model potentials employed [1]. Several model potentials have been proposed to describe interactions between CO_2 molecules [2–17]. Most of these potentials employ a simple point-charge representation of the electrostatics and neglect many-body polarization effects.

Recently, our group introduced a distributed point polarizable (DPP2) water model that accurately describes the energetics of water clusters and is also quite successful for predicting properties of bulk water [18]. In the present study, we derive a DPP2-like force field for CO_2 and apply it to small CO_2 clusters and to supercritical CO_2.

2 Methodology

2.1 Ab initio calculations

High-level electronic structure calculations on clusters have become the method of choice for parameterizing and testing force fields for condensed phase simulations of molecular structures. The symmetry-adapted perturbation theory (SAPT) [19] method has proven particularly valuable in this regard as it allows for a separation of the net interaction energy into exchange-repulsion, electrostatics, induction, and dispersion components [18]. A combination of SAPT and coupled-cluster singles-plus-doubles and perturbative triples CCSD(T) [20] calculations on small water clusters were used in the parameterization and testing of the DPP2 water model [18], and a similar strategy is employed here for developing a DPP2-like rigid-monomer force field for CO_2.

The coordinate system used for generating the ab initio data for the CO_2 dimer is described in Fig. 1. The four degrees of freedom are chosen to be the distance R between

Published as part of the special collection of articles: From quantum mechanics to force fields: new methodologies for the classical simulation of complex systems.

F.-F. Wang · R. Kumar · K. D. Jordan (✉)
Department of Chemistry and Center for Molecular and Materials Simulations, University of Pittsburgh, Pittsburgh, PA 15260, USA
e-mail: jordan@pitt.edu

Present Address:
R. Kumar
Department of Chemistry, University of Chicago, Chicago, IL 60637, USA

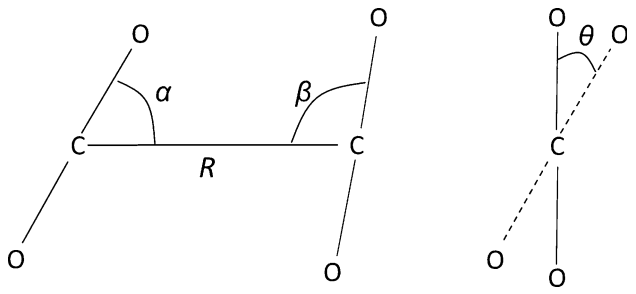

Fig. 1 Coordinates used to define the structure of the CO_2 dimers

the carbon atoms, the angles α and β between the molecular axes and the line connecting the two centers, and the dihedral angle θ. A grid of structures was generated by stepping R between 3.2 and 5.0 Å in steps of 0.3 Å and stepping each of the angles through 30 degree increments. Geometries with intermolecular O–O or C–O distances <2.7 and 2.5 Å, respectively, were excluded, leaving nearly 200 symmetry-independent dimer structures. For each of these structures, SAPT/aug-cc-pVTZ [21, 22] and CCSD(T)-F12/VTZ-F12 [23, 24] calculations were carried out. The F12 denotes the use of the explicitly correlated approach (the F12a variant) of Werner and coworkers [23], and the VTZ-F12 denotes the valence triple-zeta basis set of Peterson and coworkers [24], designed for use with the F12 method. The SAPT results were used to parameterize the electrostatics and dispersion terms in the model potential. The differences between the sum of the electrostatics, induction, and dispersion energies from the model potential and the CCSD(T)-F12/VTZ-F12 interaction energies for the dimer structures were used to fit the exchange-repulsion terms in the model potential.

The CCSD(T) three-body energies of three low-energy $(CO_2)_3$ structures shown in Fig. 2 were calculated using

$$\Delta E_3 = \sum_{i=1}^{N-2}\sum_{j=i+1}^{N-1}\sum_{k=j+1}^{N}\big[E(i,j,k) - E(i,j) - E(i,k) - E(j,k) + E(i) + E(j) + E(k)\big], \quad (1)$$

where $E(i)$, $E(i,j)$, and $E(i,j,k)$ are, respectively, the energies of the monomer i, dimer (i,j), and trimer (i,j,k) cut out of the full cluster. As discussed below, the CCSD(T)-F12/VTZ-F12 three-body interaction energies were also used in parameterizing the polarization terms in the potential.

To test the DPP2 model for CO_2, CCSD(T)-F12/VTZ-F12 interaction energies were calculated for six low-lying potential energy minima of the CO_2 dimer, trimer, and tetramer (see Fig. 2). For the dimer and trimer species, the geometries were optimized at the MP2/aug-cc-pVTZ [21, 22] level, while for the tetramer the geometry was optimized at the MP2/aug-cc-pVDZ [21, 22] level. All optimizations were carried out under the constraint of rigid monomers, with the monomer CO bond lengths and OCO angles fixed to their experimental values [25]. In addition to these minimum energy structures, 20 dimer and 20 trimer structures were randomly selected from a $T = 240$ K, $\rho = 14.9$ molecules/nm^3 *NVT* Monte Carlo simulation of supercritical CO_2 fluid to provide a further test of the model potential. These simulations were carried out using the Murthy[3] CO_2 potential, and only structures with CC distances <5 Å were retained.

The MP2 geometry optimizations and the CCSD(T)-F12 single-point calculations were performed using GAUSSIAN 03 [26] and MOLPRO [27], respectively. The SAPT calculations were carried out with the SAPT2008 [28] program interfaced with DALTON 2.0 [29]. The Monte Carlo simulations were carried out using in-house codes.

The SAPT calculations were wavefunction-based approach [19] rather than DFT based [30]. Jeziorski et al. [8] have found that the wavefunction-based SAPT procedure overestimates the dispersion of $(CO_2)_2$ near its equilibrium geometry by about 20%. However, this deficiency is largely remedied by our strategy of fitting the repulsive potential to the differences of the CCSD(T) and SAPT interaction energies.

2.2 Monte Carlo simulations

NVT Monte Carlo simulations of supercritical CO_2 as described by the DPP2 model potential were carried out for $T = 312$ K and a density of 11.4 molecules/nm^3 and for $T = 240$ K and a density of 14.9 molecules/nm^3. These conditions correspond closely to those for which radial distribution functions have been determined experimentally [31]. The simulations were carried out for 4×10^5 Monte Carlo moves following equilibration runs of 10^5 Monte Carlo steps. Each step consisted of a translation of the center of mass and a rotation of one of the monomers. The maximum values of the translational and rotational moves were optimized to give an acceptance rate of around 40%. Long-range interactions were treated with a spherical cutoff of 9.5 Å. (The interaction energy between two CO_2 molecules is negligible at distances >9.5 Å.) The same procedure was used in the Monte Carlo simulations with the Murthy potential (Table 1).

2.3 Parameterization of the model potential

2.3.1 Electrostatics

Most CO_2 model potentials represent the electrostatics by the use of three atom-centered point charges (Table 1), the values of which are chosen to reproduce the experimental quadrupole moment of the molecule. However, as seen from Table 2, such three-point-charge models give values of higher rank multipole moments very different from

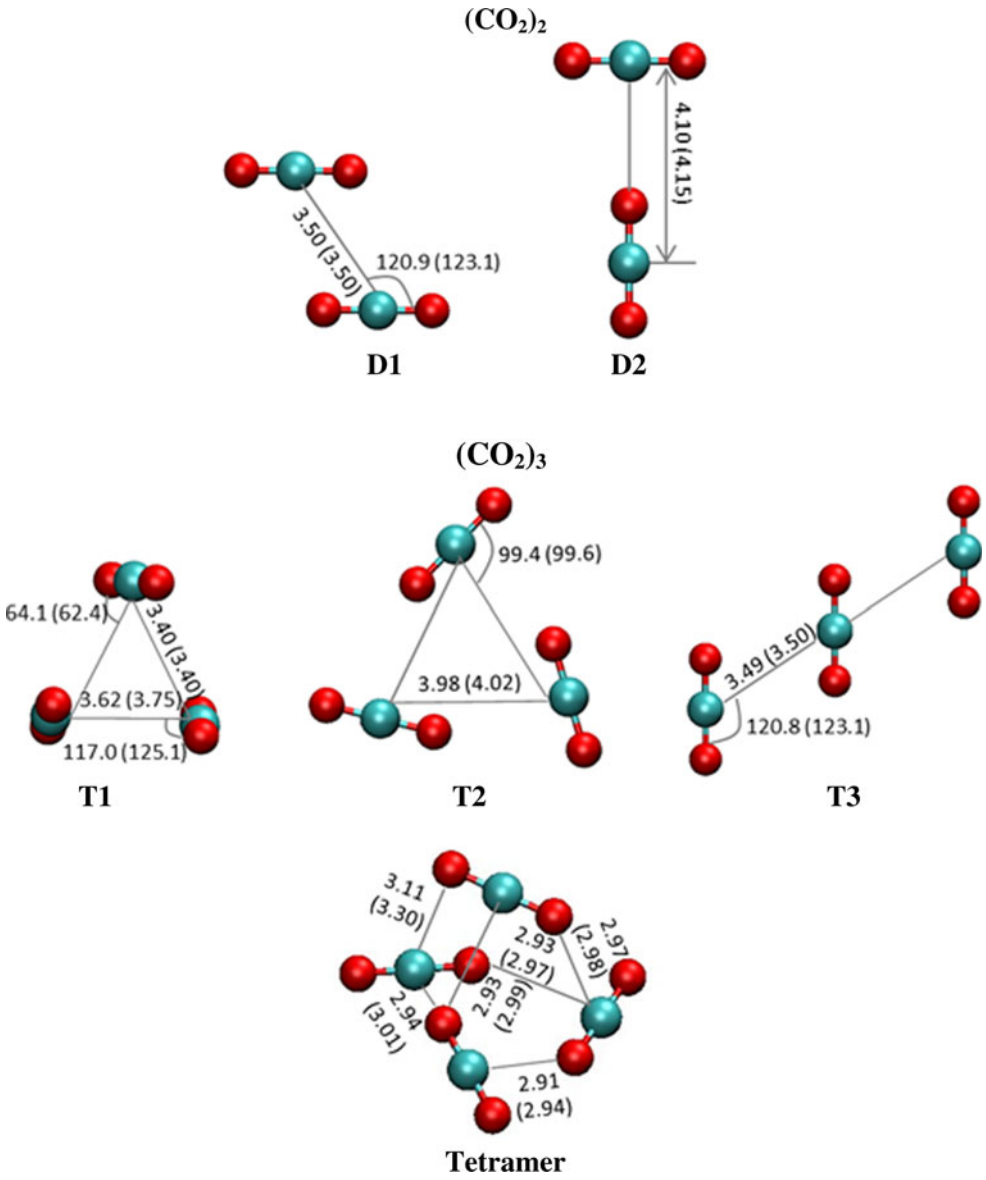

Fig. 2 The MP2 and DPP2 optimized geometries of low-energy minima of $(CO_2)_n$, $n = 2$–4 (with the DPP2 values in parenthesis, distances in Å and angles in degrees). The D2 structure for $(CO_2)_2$ is a first-order saddle point at the MP2/aug-cc-pVDZ level, but a local minimum at the MP2/aug-cc-pVTZ level

Table 1 Point charges (e), and their locations (Å) for the CO_2 models

	3-point	Murthy	DPP2
Charges			
qOn	−0.3321	−0.6418	−1.8861
qOp		0.1216	1.1971
qC	0.6642	1.0404	1.3781
Positions			
rOn	1.1599	1.0663	1.0483
rOp		1.5232	1.1599
rC	0.0	0.0	0.0

those obtained from a generalized distributed multipole analysis (GDMA) [32], analysis of the CCSD/aug-cc-pVTZ charge density of monomer. (The GDMA calculations were carried out with the ORIENT code of Stone [33].) For the minimum energy structure of the dimer, the electrostatic energy calculated using the moments through rank 4 is −0.87 kcal/mol, while that obtained from a three-point-charge model, with the charges chosen as described above, is only −0.49 kcal/mol. Clearly, the higher rank moments play an important role in the electrostatic interactions between CO_2 molecules.

Murthy's CO_2 model [3] employs five-point charges, one on the C atom and one on each side of each O atom, all located on the molecular axis. This leads to an improved description of the higher multipole moments and gives a value of −0.76 kcal/mol for electrostatic interaction energy of the dimer at its global minimum structure, in improved agreement with the GDMA result. Our DPP2-like model also employs five-point charges, but with three atom-

Table 2 Multipole moments (a.u.) of CO_2 from various models and from a GDMA analysis of the CCSD/aug-cc-pVTZ charge density and electrostatic energies (kcal/mol) of the $(CO_2)_2$ potential energy minimum

Moments	Approach			
	3-point	Murthy	DPP2	Ab initio
Rank2	−3.20	−3.20	−3.30	−3.30[a]
Rank4	−15.33	−4.47	−2.83	−2.85[a]
Rank6	−73.66	52.40	37.52	27.92[a]
Rank8	−353.88	797.20	380.88	387.85[a]
ES	−0.49	−0.76	−0.88	−0.87[b]

[a] Calculated with GDMA using CCSD/aug-cc-pVTZ charge density

[b] Calculated with ORIENT using atomic moments obtained by GDMA through rank 4. Thus this contribution does not include charge penetration

centered charges and additional off-atom charges located near each of the O atoms. The values of the charges and the locations of the off-atom charges were optimized by a least-square fitting to the electrostatic potential calculated at the CCSD/aug-cc-pVTZ level, constraining the quadrupole moment to the CCSD value of −3.30 a.u. The regions within 2.55 and 2.43 Å of the C and O nuclei, respectively, were excluded in the fitting. The results are summarized in Table 2, from which it is seen that the DPP2 model for CO_2 does significantly better than both the 3-point model and Murthy's 5-point model at reproducing the higher multipole moments and at representing the non-charge-penetration [34] portion of the electrostatic interaction energy in the CO_2 dimer.

To account for the short-range charge penetration portion of the electrostatics interaction between two CO_2 molecules, an approximation introduced by of Freitag et al. [35] is employed. This express the penetration energy as

$$E_{pen} = -\frac{1}{2R_{AB}}\left[q_A(q_B+2Z_B)e^{-a_AR_{AB}} + q_B(q_A+2Z_A)e^{-a_BR_{AB}} + \frac{q_Aq_B\left(a_A^2+a_B^2\right)}{a_A^2-a_B^2}\left(e^{-a_BR_{AB}}-e^{-a_AR_{AB}}\right)\right], \quad (2)$$

in the case that A and B refer to different types of charge sites, and

$$E_{pen} = -\frac{1}{R_{AB}}\left[q_Aq_B\left(1+\frac{aR_{AB}}{2}\right)+q_AZ_B+q_BZ_A\right]e^{-aR_{AB}}, \quad (3)$$

when A and B refer to the same type of site (i.e., C–C, O–O, or off-atom–off-atom).

In Eqs. 2 and 3, Z_A and Z_B are the numbers of valence electrons associated with atoms A and B, respectively, that is, six for O, four for C, and zero for off-atom sites, and q_A and q_B are the point charges employed in the model. The a parameters, obtained by least-squares fitting

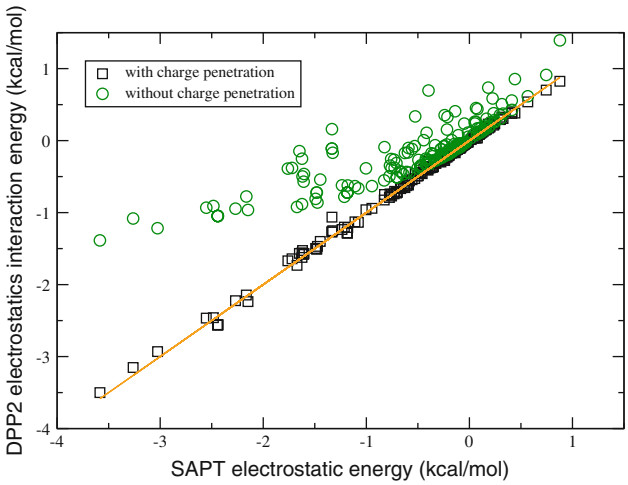

Fig. 3 Electrostatic interaction energies for the dimer training set

the electrostatic energy potential from the SAPT calculations on the ~200 CO_2–CO_2 dimer structures, are 0.35215, 0.40174, and 0.32296 $Å^{-1}$ for C, O, and off-atom sites, respectively.

Figure 3 reports, for the CO_2 dimer training set, the electrostatic energies obtained using the DPP2 5-point charge model with and without charge penetration as well as the electrostatic energies from SAPT calculations. It is seen that the DPP2 5-point charge model with the charge penetration correction closely reproduces the electrostatic interaction energies from the SAPT calculations.

2.3.2 *Polarization*

The polarization interactions are modeled using mutually interacting atom-centered point polarizable sites, with Thole-type [36] damping between the charges and induced dipoles and between the induced dipoles. The procedure used to calculate the polarization energy is described in [18]. The atomic polarizabilities of CO_2 and the dipole–dipole damping coefficient were chosen so that the model gives $\alpha_{\parallel}$ and $\alpha_{\perp}$ polarizability components of CO_2 close to the experimental values [37]. The values of the charge-induced dipole damping coefficient was determined so that the model potential gives three-body energies for the three local minima of the $(CO_2)_3$ cluster close to those obtained from the CCSD(T) calculations. The resulting parameters are summarized in Table 3, and the resulting molecular polarizabilities and 3-body energies are reported in Tables 4 and 5, respectively. As noted by other researchers [8, 15], the 3-body interactions are quite small (≤0.1 kcal/mol in magnitude) for the CO_2 trimer.

Figure 4 compares, for the CO_2–CO_2 dimers in the training set, the polarization energies from the DPP2 model with the induction energies from the SAPT calculations, from which it is seen that for many of the sampled

Table 3 Atomic polarizabilities and damping parameters used for describing polarization in the DPP2 model of CO_2

Polarizability	
α_C (Å^3)	1.35
α_O (Å^3)	0.90
Damping parameters[a]	
a_{cd}	0.16
a_{dd}	0.65

[a] a_{cd} and a_{dd} refer to the damping parameters in the charge-induced dipole and induced dipole-induced dipole terms, respectively

Table 4 Molecular polarizability (Å^3) of the carbon dioxide monomer

	α_{xx}	α_{zz}	$\overline{\alpha}$
MP2[a]	1.91	4.04	2.65
CCSD(T)[a]	1.89	3.94	2.61
DPP2	1.93	3.88	2.58
Experiment[b]	1.91	3.94	2.59

[a] with aug-cc-pVTZ basis set

[b] [37]

Table 5 Three-body energies (kcal/mol) of local minima $(CO_2)_3$

Method	T1	T2	T3
DF-MP2/aug-cc-pV5Z	−0.04	−0.12	0.03
CCSD(T)-F12/VTZ-F12	0.01	−0.12	0.02
DPP2	−0.03	−0.12	0.02

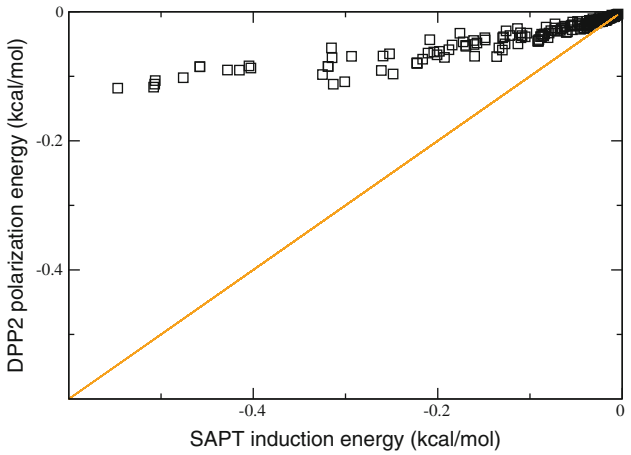

Fig. 4 Induction energies for CO_2 dimer training set calculated using the DPP2 model and the SAPT procedure

configurations the 2-body polarization energies from the DPP2 model significantly underestimate the 2-body induction energies from SAPT calculations. We note that the implementation of the DPP2 model for CO_2 neglects charge-transfer, which an ALMO EDA [38] analysis indicates is in the order of −0.1 kcal/mol for the most stable dimer structure. In addition, the distributed inducible dipoles of the DPP2 model do a poor job at representing the quadrupole–quadrupole polarizability of the CO_2 monomer, which we estimate, if properly treated, contributes ∼−0.05 kcal/mol to the induction energy of the D1 dimer. We further note that charge penetration effects can enhance rather than attenuate induction energies [39]. In any case, the 2-body induction energies are far less important than the electrostatics and dispersion contributions, being at most −0.54 kcal/mol, and, to a large extent, the deficiency of the model in describing the induction is compensated for by the procedure used to fit the repulsion contributions.

2.3.3 Dispersion

The dispersion interactions between pairs of monomers are represented by damped r_{ij}^{-6} terms, that is, as

$$E_{disp} = \sum_{i,j} \frac{C_6^{ij} f(r_{ij}, \delta_{ij})}{r_{ij}^6}, \tag{4}$$

where i and j refer to atoms of different monomers, and $f(r_{ij}, \delta_{ij})$ is the Tang-Toennies damping function [40]. The $C_6^{ij}$and δ_{ij} parameters (summarized in Table 6) were obtained by fitting to the SAPT values of the dispersion energies (sum of dispersion plus exchange-dispersion) for the set of CO_2–CO_2 dimer structures. As seen from Fig. 5, the SAPT values of the dispersion energies for the CO_2–CO_2 dimers in the training set are well represented by the DPP2 model.

2.3.4 Exchange–repulsion

The 2-body exchange-repulsion interactions are represented as

$$E_{exch-rep} = \sum_{i,j} A_{ij} \exp(-B_{ij} r_{ij}), \tag{5}$$

where i and j refer to atoms associated with different monomers. The A_{ij} and B_{ij} parameters (summarized in Table 6) were determined by fitting for the CO_2–CO_2 dimer training set the residual energies obtained by subtracting for

Table 6 Parameters describing the dispersion and repulsion interactions in the DPP2 model for CO_2

Atoms	Dispersion		Repulsion	
	C_6^{ij} (kcal/mol Å^6)	δ_{ij} (Å^{-1})	A_{ij} (kcal/mol)	B_{ij} (Å^{-1})
C–C	−97.76	31.326	0.674764	0.67716
C–O	−288.57	33.307	6,727.82	3.0016
O–O	−497.23	28.026	240,059.0	4.22009

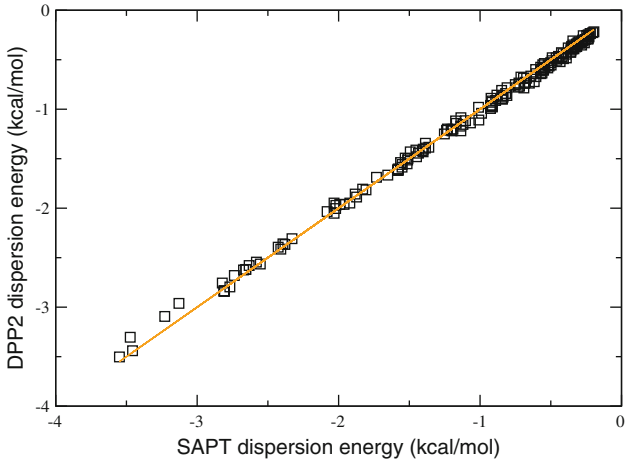

Fig. 5 Dispersion interaction energies for CO_2 dimer training set calculated using the model potential and the SAPT procedure

each structure the sum of the DPP2 values of the electrostatics, polarization, and dispersion energies from the CCSD(T)-F12 interaction energies. As noted above, this approach ensures that deficiencies in the model for describing the electrostatics, induction, and dispersion energies are partially compensated for by the so-called exchange–repulsion term. It is seen from Fig. 6 that the DPP2 model accurately reproduces the CCSD(T)-F12 values of the net interaction energies of the $(CO_2)_2$ training set.

3 Testing the DPP2 model

3.1 $(CO_2)_n$ ($n = 2$–4)

The geometries of the stationary points of the $(CO_2)_n$, $n = 2$–4 clusters obtained from MP2 and DPP2 optimizations are shown in Fig. 2, and the calculated interaction energies are summarized in Table 7. From Fig. 2 it is seen that the DPP2 model gives geometries very close to those from the MP2 optimizations. As seen from Table 7, the DPP2 model also closely reproduces the CCSD(T)-F12 interaction energies of these clusters with the mean absolute error being <0.1 kcal/mol. In contrast, for the Murthy model the mean absolute error in the interaction energies for the $(CO_2)_n$, $n = 2$–4 clusters is nearly 0.5 kcal/mol.

Table 7 Interaction energies (kcal/mol) of selected stationary points $(CO_2)_n$, $n = 2$–4

Method	$(CO_2)_2$		$(CO_2)_3$			$(CO_2)_4$
	D1	D2	T1	T2	T3	
MP2-F12[a]	−1.46	−1.20	−3.97	−3.83	−2.93	−7.26
CCSD(T)-F12[a]	−1.50	−1.23	−3.99	−3.94	−3.03	−7.33
DPP2[a]	−1.52	−1.13	−4.05	−3.73	−3.07	−7.26
Murthy[a]	−1.34	−1.03	−3.57	−3.25	−2.73	−6.36
DPP2 (opt)[b]	−1.56	−1.14	−4.17	−3.74	−3.15	−7.41

[a] Results for MP2 optimized geometries

[b] Results for DPP2 optimized geometries

Figure 7 reports for dimer and trimer structures sampled in the $T = 240$ K Monte Carlo simulation, the interaction energies obtained using DPP2 and Murthy models as well as from the CCSD(T)-F12 method. The DPP2 model accurately reproduces the interaction energies from the CCSD(T)-F12 calculations, with the maximum error being about 0.2 kcal/mol. The Murthy model also performs well for structures with large intermolecular separations; however, it is less successful for structures with small intermolecular separations.

One question that can be raised about the DPP2 model is the appropriateness of including many-body polarization

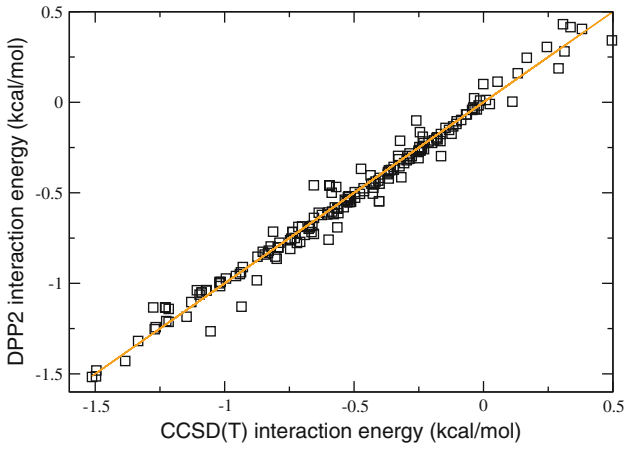

Fig. 6 Net interaction energies for the CO_2 dimer training set calculated using the DPP2 model potential and the CCSD(T)-F12 method

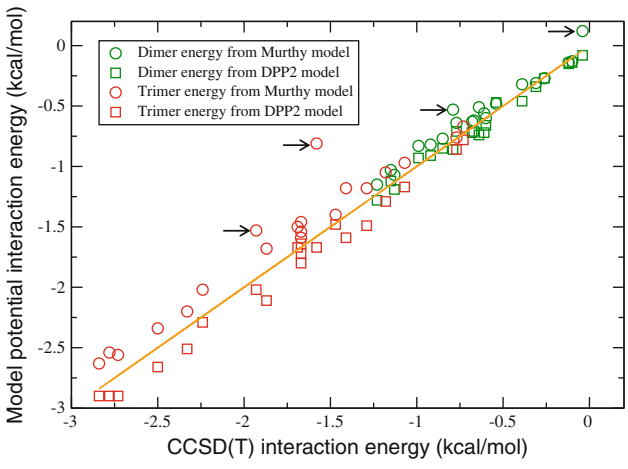

Fig. 7 Net interaction energies for a set of dimer and trimer structures sampled in a $T = 240$ K Monte Carlo simulation. *Arrows* indicate structures with intermolecular O–O distances shorter than 2.9 Å

effects while ignoring many-body dispersion interactions. To address this issue, we have carried out 3-body SAPT [41] calculations on the global minimum structure of $(CO_2)_3$. These calculations give the following three-body contributions, exchange (−0.04 kcal/mol), induction, including the δ(HF) contribution (−0.01 kcal/mol), and dispersion (0.24 kcal/mol) for a net 3-body contribution of 0.20 kcal/mol, compared to the CCSD(T) value of 0.01 kcal/mol. Thus, although the dispersion contribution is largest in magnitude, all these contributions to the 3-body energy are small compared to the net interaction energy. In addition, it should be noted that the DPP2 model gives a 3-body interaction energy of −0.03 kcal/mol, very close to the CCSD(T) value. Indeed, the way the DPP2 model was parameterized the so-called 3-body polarization contribution can be thought of as effectively incorporating exchange and dispersion interactions as well.

3.2 Second virial coefficient

The second virial coefficient is a basic thermodynamic quantity that represents the departure from ideality due to interactions between pairs of molecules. The second virial coefficient as a function of temperature for the DPP2-like CO_2 model was calculated by numerically integrating the Mayer function [42]:

$$B_2(T) = -2\pi \int_0^\infty \left[\langle e^{-\beta u(r)}\rangle - 1\right] r^2 dr, \qquad (2)$$

where the average of $e^{-\beta u(r)}$was taken over randomly sampled molecular orientations at a fixed intermolecular distance r. Calculated and measured [43] B_2 versus T curves are reported in Fig. 8. It is seen that the DPP2 force field for CO_2 gives values of the second virial coefficients in excellent agreement with experiment.

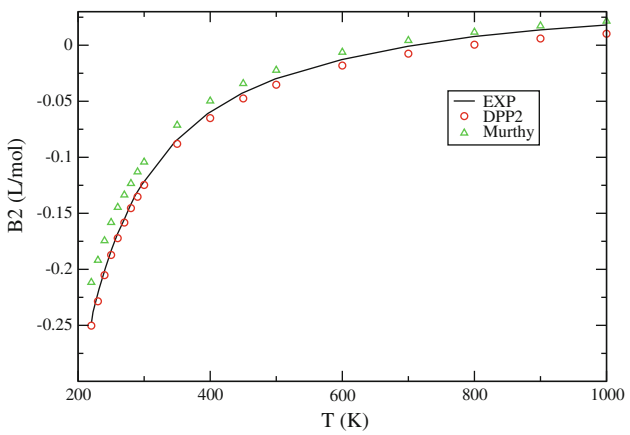

Fig. 8 Calculated and experimental [43] second virial coefficient for CO_2

3.3 Supercritical CO_2

Radial distribution functions (RDF) available for supercritical CO_2 are available from neutron diffraction studies [31]. These experientially determined RDFs do not resolve the contributions for the various atom pairs. Thus to enable comparison with experiment we have calculated atom–atom partial radial distribution functions using the expression

$$g_m(r) = 0.403 g_{oo}(r) + 0.464 g_{co}(r) + 0.133 g_{cc}(r) \qquad (6)$$

from [44]. This expression accounts for the difference in the neutron scattering cross sections of C and O. As seen from Fig. 9, for both sets of conditions ($T = 240$ K, $\rho = 14.9$ molecules/nm^3 and $T = 312$ K, $\rho = 11.4$ molecules/nm^3), the radial distribution functions calculated using the DPP2 force field for CO_2 are in excellent agreement with those determined experimentally.

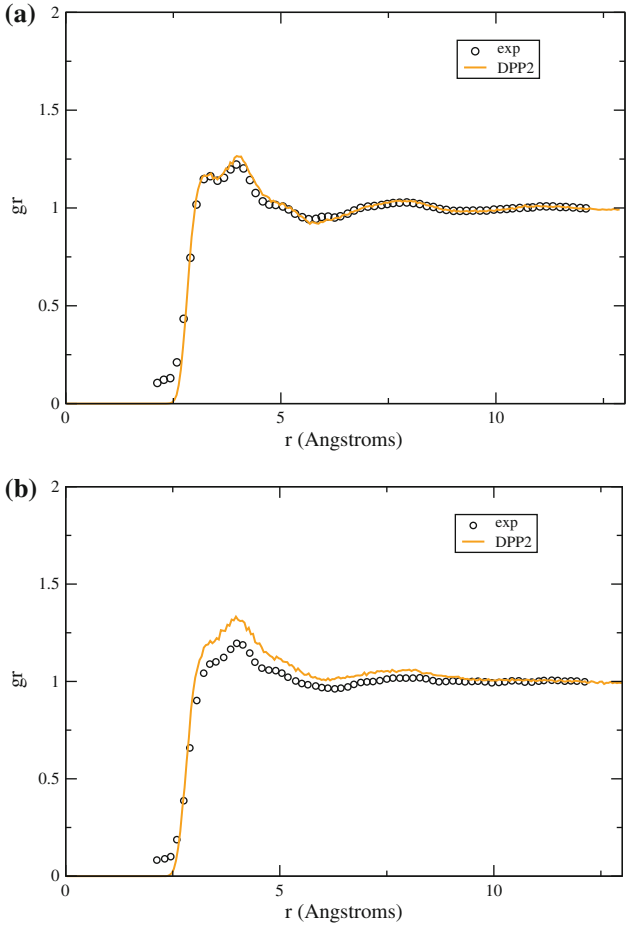

Fig. 9 Radial distribution function of supercritical CO_2. **a** calculated and experimental results for $T = 240$ K and $\rho = 14.9$ molecules/nm^3 **b** calculated and experimental results for $T = 312$ K and $\rho = 11.4$ molecules/nm^3. The experimental results are from [31]

4 Conclusions

In this study, we have constructed a CO_2 force field using the same strategy as used previously to develop the DPP2 water model, that is, using a combination of SAPT and CCSD(T) calculations to fit individual electrostatic, induction, dispersion, and exchange–repulsion contributions. The resulting DPP2-like force field of CO_2 is shown to accurately reproduce the MP2 geometries and the CCSD(T)-F12 interaction energies of small $(CO_2)_n$ clusters and also to give second virial coefficient values and radial distribution functions of supercritical CO_2 in excellent agreement with experiment. In future work we plan to extend the DPP2 model to describe CO_2-water interactions, to enable its use in simulations of CO_2-liquid water mixtures and of CO_2 hydrates.

Acknowledgments This research was carried out with the support of the National Science foundation, grant CHE 518253. The calculations were carried out on computers in the University of Pittsburgh's Center for Simulation and Modeling.

References

1. MacKerell AD Jr (2001) Atomistic models and force fields. In: Becker OM, MacKerell AD Jr, Roux B, Watanabe M (eds) Computational biochemistry and biophysics. Marcel Dekker Inc, New York
2. Murthy CS, Singer K, McDonald IR (1981) Mol Phys 44:135
3. Murthy CS, O'Shea SF, Mcdonald IR (1983) Mol Phys 50:531
4. Böhm HJ, Meissner C, Ahlrichs R (1984) Mol Phys 53:651
5. Zhu SB, Robinson GW (1989) Comput Phys Commun 52:317
6. Etters RD, Kuchta B (1989) J Chem Phys 90:4537
7. Möller D, Fischer J (1994) Fluid Phase Equilib 100:35
8. Bukowski R, Sadlej J, Jeziorski B, Jankowski P, Szalewicz K, Kucharski SA, Williams HL, Rice BM (1999) J Chem Phys 110:3785
9. Bock S, Bich E, Vogel E (2000) Chem Phys 257:147
10. Potoff JJ, Siepmann JI (2001) AIChE J 47:1676
11. Vrabec J, Stoll J, Hasse H (2001) J Phys Chem B 105:12126
12. Zhang Z, Duan Z (2005) J Chem Phys 122:214507
13. Zhu A, Zhang X, Liu Q, Zhang Q (2009) Chin J Chem Eng 17:268
14. Merker T, Engin C, Vrabec J, Hasse H (2010) J Chem Phys 132:234512
15. Oakley MT, Wheatley RJ (2009) J Chem Phys 130:034110
16. Persson RAX (2011) J Chem Phys 134:034312
17. Yu K, McDaniel JG, Schmidt JR (2011) J Phys Chem B 115:10054
18. Kumar R, Wang F–F, Jenness GR, Jordan KD (2010) J Chem Phys 132:014309
19. Jeziorski B, Moszynski R, Szalewicz K (1994) Chem Rev 94:1887
20. Purvis GD, Bartlett RJ (1982) J Chem Phys 76:1910
21. Kendall RA, Dunning TH, Harrison RJ (1992) J Chem Phys 96:6796
22. Woon DE, Dunning TH (1994) J Chem Phys 100:2975
23. Adler TB, Knizia G, Werner H-J (2007) J Chem Phys 127:221106
24. Peterson KA, Adler TB, Werner H-J (2008) J Chem Phys 128:084102
25. Eggenberger R, Gerber S, Huber H (1991) Mol Phys 72:433
26. Frisch MJ, Trucks GW, Schlegel HB, Scuseria GE, Robb MA, Cheeseman JR, Montgomery Jr. JA, Vreven T, Kudin KN, Burant JC, Millam JM, Iyengar SS, omasiJT, aroneVB, Mennucci B, Cossi M, Scalmani G, Rega N, Petersson GA, Nakatsuji H, Hada M, Ehara M, Toyota K, Fukuda R, Hasegawa J, Ishida M, Nakajima T, Honda Y, Kitao O, Nakai H, Klene M, Li X, Knox JE, Hratchian HP, Cross J B, Bakken V, Adamo C, Jaramillo J, Gomperts R, Stratmann RE, Yazyev O, Austin AJ, Cammi R, Pomelli C, Ochterski JW, Ayala PY, Morokuma K, Voth GA, Salvador P, Dannenberg JJ, Zakrzewski VG, apprichSD, Daniels AD, Strain MC, Farkas O, Malick DK, Rabuck AD, Raghavachari K, Foresman JB, Ortiz JV, Cui Q, Baboul AG, Clifford S, Cioslowski J, Stefanov BB, Liu G, Liashenko A, Piskorz P, Komaromi I, Martin RL, Fox DJ, Keith T, Al-Laham MA, Peng CY, Nanayakkara A, Challacombe M, Gill PMW, Johnson B, Chen W, Wong MW, Gonzalez C, Pople JA (2004) Gaussian 03, Revision C.02, Gaussian, Inc, Wallingford, CT
27. Werner H-J, Knowles PJ, Lindh R, Manby FR, Schütz M, Celani P, Korona T, Rauhut G, Amos RD, Bernhardsson A, Berning A, Cooper DL, Deegan MJO, Dobbyn AJ, Eckert F, Hampel C, Hetzer G, Lloyd AW, McNicholas SJ, Meyer W, Mura ME, Nicklass A, Palmieri P, Pitzer R, Schumann U, Stoll H, Stone AJ, Tarroni R, Thorsteinsson T, MOLPRO, version 2006.1, a package of ab initio programs. http://www.molpro.net
28. Bukowski R, Cencek W, Jankowski P, Jeziorska M, Jeziorski B, Kucharski SA, Lotrich VF, Misquitta AJ, Moszyński R, Patkowski K, Podeszwa R, Rybak S, Szalewicz K, Williams HL, Wheatley RJ, Wormer PES, Żuchowski PS, SAPT2008: An Ab Initio Program for Many-Body Symmetry-Adapted Perturbation Theory Calculations of Intermolecular Interaction Energies, University of Delaware and the University of Warsaw
29. DALTON, a molecular electronic structure program, Release 20 (2005). http://www.kjemi.uio.no/software/dalton/dalton.html
30. Misquitta AJ, Podeszwa R, Jeziorski B, Szalewicz K (2005) J Chem Phys 123:214103
31. Cipriani P, Nardone M, Ricci FP (1998) Phys B 241–243:940
32. Stone AJ (2005) J Chem Theory Comput 1:1128
33. Stone AJ, Dullweber A, Engkvist O, Fraschini E, Hodges MP, Meredith AW, Nutt DR, Popelier PLA, Wales DJ (2002) 'Orient: a program for studying interactions between molecules, version 45,' University of Cambridge, Enquiries to Stone AJ, ajs1@cam.ac.uk
34. Stone AJ (1996) The theory of intermolecular forces. Clarendon, Oxford
35. Freitag MA, Gordon MS, Jensen JH, Stevens WJ (2000) J Chem Phys 112:7300
36. Thole BT (1981) Chem Phys 59:341
37. Maroulis G, Thakkar AJ (1990) J Chem Phys 93:4164
38. Khaliullin RZ, Cobar EA, Lochan RC, Bell AT, Head-Gordon M (2007) J Phys Chem A 111:8753
39. Wang B, Thuhlar DG (2010) J Chem Theory Comput 6:3330
40. Tang KT, Toennies JP (1984) J Chem Phys 80:3726
41. Podeszwa R, Szalewicz K (2007) J Chem Phys 126:194101
42. McQuarrie DA (2000) Statistical mechanics. University Science Books
43. Span R, Wagner W (1996) J Phys Chem Ref Data 25:1509
44. Ishii R, Okazaki S, Odawara O, Okada I, Misawa M, Fukunaga T (1995) Fluid Phase Equilibria 104:291